Phage-Display-Guided Nanocarrier Targeting to Atheroprone Vasculature

Lucas H. Hofmeister,[†] Sue Hyun Lee,[†] Allison E. Norlander,[‡] Kim Ramil C. Montaniel,[‡] Wei Chen,[‡] David G. Harrison,*[,†,‡,§,∥] and Hak-Joon Sung*[,†,∥]

[†]Department of Biomedical Engineering, [‡]Division of Clinical Pharmacology, [§]Center for Vascular Biology, and [∥]Division of Cardiovascular Medicine, Vanderbilt University, Nashville, Tennessee 37235, United States

ABSTRACT In regions of the circulation where vessels are straight and unbranched, blood flow is laminar and unidirectional. In contrast, at sites of curvature, branch points, and regions distal to stenoses, blood flow becomes disturbed. Atherosclerosis preferentially develops in these regions of disturbed blood flow. Current therapies for atherosclerosis are systemic and may not sufficiently target these atheroprone regions. In this study, we sought to leverage the alterations on the luminal surface of endothelial cells caused by this atheroprone flow for nanocarrier targeting. *In vivo* phage display was used to discover unique peptides that selectively bind to atheroprone regions in the mouse partial carotid artery ligation model. The peptide GSPREYTSYMPH (PREY) was found to bind 4.5-fold more avidly to the region of disturbed flow and was used to form targeted liposomes. When administered intravenously, PREY-targeted liposomes preferentially accumulated in endothelial cells in the partially occluded carotid artery and other areas of disturbed flow. Proteomic analysis and immunoblotting indicated that fibronectin and Filamin-A were preferentially bound by PREY nanocarriers in vessels with disturbed flow. In additional experiments, PREY nanocarriers were used therapeutically to deliver the nitric oxide synthase cofactor tetrahydrobiopterin (BH_4), which we have previously shown to be deficient in regions of disturbed flow. This intervention increased vascular BH_4 and reduced vascular superoxide in the partially ligated artery in wild-type mice and reduced plaque burden in the partially ligated left carotid artery of fat fed atheroprone mice ($ApoE^{-/-}$). Targeting atheroprone sites of the circulation with functionalized nanocarriers provides a promising approach for prevention of early atherosclerotic lesion formation.

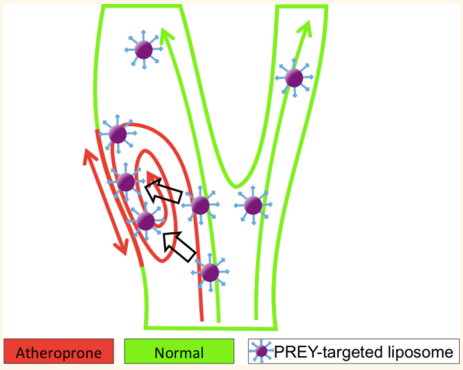

KEYWORDS: phage display · liposome · disturbed flow atherosclerosis · tetrahydrobiopterin

Arterial geometry affects the blood flow profiles in the cardiovascular system. In straight, unbranched vascular segments, blood flow is unidirectional and laminar and time average wall shear stress is high. In contrast, at branch points, sites of curvature, and distal to stenoses, blood flow becomes disturbed. Such regions can display flow separation, vortical shedding, and low and oscillatory shear stresses.[1] The vascular endothelium is in direct contact with flowing blood and displays remarkable plasticity in response to varying shear stresses.[2] In the setting of unidirectional laminar shear stress, endothelial cells elongate and align in the direction of flow and develop an anti-inflammatory and antithrombotic phenotype.[3] These effects are associated with acute changes in endothelial cell signaling and marked changes in gene expression over the long-term.[2,4] As examples, in response to laminar shear, endothelial cells increase nitric oxide (NO) and endothelial nitric oxide synthase (eNOS) and exhibit decreases in inflammatory mediators.[5] In striking contrast, endothelial cells exposed to disturbed flow do not align and elongate and become pro-inflammatory and pro-thrombotic. This phenotype is associated with sustained activation of pro-inflammatory signals with increased expression of inflammatory mediators including vascular cell adhesion molecule-1, intracellular adhesion molecule-1, and chemokines such as the monocyte chemoattractant peptide-1.[3,6−9] The changes in endothelial cell phenotype caused by disturbed flow predispose these regions to local lipid deposition, inflammation, and the focal development of atherosclerosis. Thus, atherosclerotic lesions predominantly occur at sites known to have oscillatory shear stress such as branch points, the proximal coronary arteries, and the distal aorta.[6,7,10]

* Address correspondence to hak-joon.sung@vanderbilt.edu, david.g.harrison@vanderbilt.edu.

Received for review February 13, 2015 and accepted March 13, 2015.

Published online March 13, 2015
10.1021/acsnano.5b01048

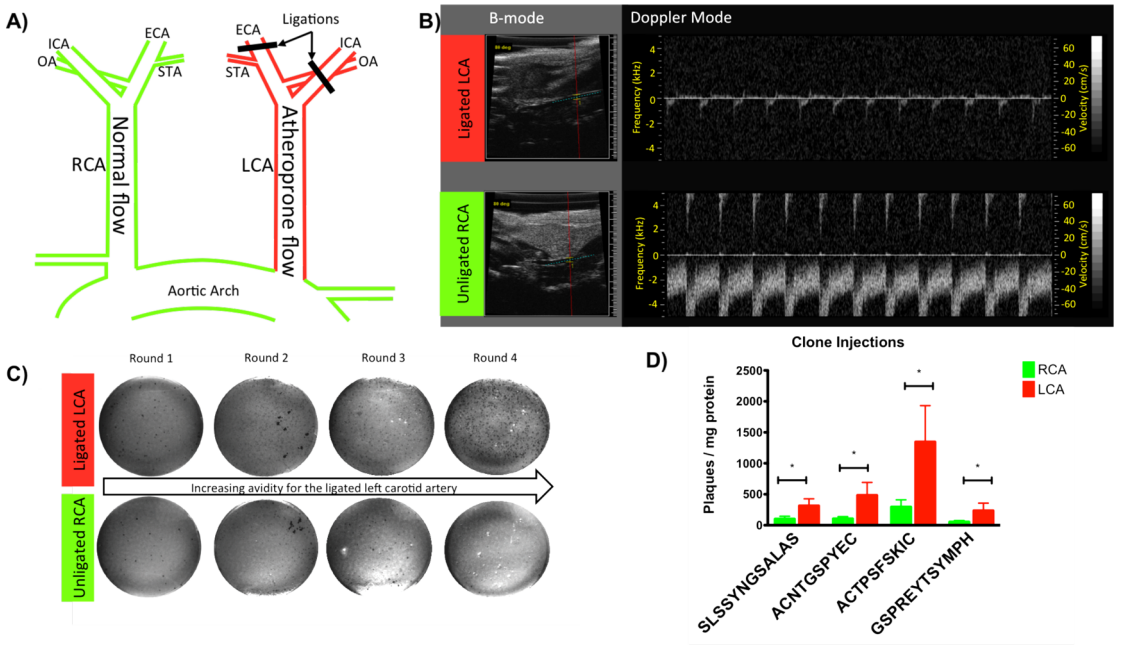

Figure 1. *In vivo* **phage display methods and results. (A) Schematic of the partial carotid artery ligation surgery. (B) Ultrasound demonstrating low velocity atheroprone flow and flow reversal in the ligated LCA (top) and normal pulsatile and unidirectional flow in the unligated RCA (bottom). (C)** *In vivo* **phage display titration results. (D) Clone injection titration demonstrates that all phage clones result in significantly greater binding to the ligated LCA; *$p < 0.05$ between the RCA and LCA.**

Most current treatments for atherosclerosis focus on correcting systemic risk factors such as hyperlipidemia, hypertension, and diabetes. None of these therapies completely prevents cardiovascular events resulting from atherosclerosis. As an example, HMG Co-A reductase inhibitors reduce cardiovascular events by approximately 40 to 50%, indicating that there are residual risks that persist after lipid lowering.[11,12] One explanation of this residual risk is that current treatments do not target vasculature that is atheroprone, and such regions might require high local doses of drug not achieved by systemic administration.

Nanocarriers are an attractive platform for targeting therapy to regions of the circulation at risk for atherosclerosis. Nanoparticles can be functionalized to home to specific vascular regions affected by inflammation, lipid accumulation, or oxidative injury and can be used to deliver either therapeutic or imaging agents. Previously, nanoparticles have been used that target inflamed endothelium, inflammatory cells, the low-density lipoprotein receptor, thrombi, and platelet aggregates.[13−20] While these studies have set a precedent for nanoparticle delivery to atherosclerosis, they depend on the presence of lesions formed after the initiation of the disease.

In the present study, we sought to develop a novel nanotherapy to target atheroprone regions of the circulation prior to atherosclerotic lesion development. Given the marked differences in gene expression and protein content of endothelial cells exposed to varying flow profiles, we reasoned that there might be a difference in peptide binding to the surface of cells exposed to disturbed *versus* unidirectional laminar shear. Using combinatorial phage display, we identified peptides that preferentially accumulate in an area of disturbed flow created by partial carotid occlusion in mice. A candidate peptide identified in this screen was used to functionalize liposomal nanocarriers. Subsequent studies proved that these nanocarriers also targeted regions of disturbed flow and could be used to deliver effective anti-atherosclerotic therapy to these regions.

RESULTS AND DISCUSSION

In vivo phage panning was performed in the partial carotid artery ligation model of disturbed flow in male C57/BL6J mice.[9,21] In this surgical model, three of the four major branches of the left common carotid artery (LCA) are ligated (Figure 1A). This results in low and oscillatory flow in the LCA, while flow in the right common carotid artery (RCA) remains normal. Doppler ultrasound imaging confirmed disturbed blood flow in the ligated LCA and normal blood flow in the sham RCA 1 day after ligation (Figure 1B). The ligated left carotid artery is the target for phage display, while the right artery serves as a normal flow control.

Four days postligation, *in vivo* phage display was carried out. Two peptide libraries were employed for screening, a linear 12 amino acid, and a cyclic 7 amino acid library (New England Biolabs, Ipswich, MA). Phages were injected into the tail vein of the mice at a concentration of 2×10^{11} plaque-forming units. After 2.5 h, mice were sacrificed by CO_2 inhalation, and the carotid arteries were surgically isolated; phages were

TABLE 1. Protein Homology of Phage-Displayed Consensus Peptides

sequence	name	identity sequence	accession no.
GSPREYTSYMPH	myoferlin	496-SPREYT-501	NP_001093104
SLSSYNGSALAS	eyes absent homologue 1 isoform 2	27-SLDSFSGSALGS-38	NP_001239121
ACNTGSPYEC	zinc finger protein	160-CHTGEKPYEC-169	AAA64428
ACTPSFSKIC	calsyntenin 1, isoform CRA_b	187-CSPQFSQIC-195	EDL14871

recovered from the vessels. To increase stringency of the screening process and specificity of the phages for the target condition, arteries were washed with acidic buffer to remove weakly bound phages, and the remaining phages were recovered by cell lysis and amplified in bacteria. These phages were then re-injected in other mice with partial carotid ligation. This strategy of using successive rounds of injection, isolation by cell lysis, and reamplification has been used previously to isolate phages that are internalized by target cells.[17] Selecting ligands that could mediate nanoparticle internalization into target cells is desired when cytoplasmic delivery of a drug is necessary and helps to increase the signal for imaging applications. After each round of phage display, titration of the phage recovered from the arteries was used to quantify relative uptake in the target LCA and control RCA. After each round, phages isolated from the target LCA were amplified, purified, and reinjected for the subsequent round of phage display.

Figure 1C shows examples of phage isolations following each round of injections. From round one to round four, there was a progressive increase in the number of phages binding to the target LCA (top) and no increase in binding to the RCA (bottom). The increased binding to the target LCA indicated that clones were being selected that preferentially accumulated in vessels exposed to disturbed flow. After round three and four of phage screening, 10 plaques from titration plates were sequenced. Four peptide sequences were identified as dominating those that selectively accumulated in the regions of disturbed flow (Table 1). Two of these encoded linear 12 amino acid peptides are SLSSYNGSALAS and GSPREYTSYMPH. Two sequences that encoded 7 amino acid cyclic peptides were also identified, ACNTGSPYEC and ACTPSFSKIC. Protein BLAST was used to identify potential protein interactions (Table 1).

In additional experiments, we amplified and injected these consensus clones following the same procedures as *in vivo* phage library panning. Titration of phage normalized to the protein content of the corresponding LCA or RCA was used to determine the relative uptake between the target and control arteries. All four consensus clones showed a significantly increased binding to the targeted LCA. ACTPSFSKIC showed average enrichment of 7.3-fold; SLSSYNGSALAS showed enrichment of 4.9; ACNTGSPYEC showed enrichment of 6.1, and GSPREYTSYMPH showed enrichment of 4.4 in the target artery (Figure 1D). In addition, when these phages were injected into mice that had undergone a sham surgery 4 days previously, they did not accumulate differently between the LCA and RCA, indicating that the consensus clones do not target the LCA in the absence of disturbed flow. These experiments confirmed that the consensus peptides discovered in the initial screen specifically accumulate in regions of disturbed flow.

The phage-displayed peptide GSPREYTSYMPH (PREY) was chosen as a candidate for initial studies due to its ease of synthesis, hydrophilicity, neutral charge, and homology to murine myoferlin and because it showed the lowest level of binding to the right carotid artery. Myoferlin has regulatory roles in endothelial cells as it is critical for endocytosis, regulates vascular endothelial growth factor receptor-2 stability and function, and is implicated in endothelial membrane repair.[22−24] In addition, myoferlin is enriched in caveolae, which are also implicated in endothelial cell response to shear stress.[25,26]

To determine the binding partner for the PREY peptide, we employed a pull-down followed by proteomics analysis. The phage-displayed peptide acetyl-GSPREYTSYMPHGSGS-COOH (PREY) and the scrambled control peptide acetyl-THRPMSSYEPGYGSGS-COOH (scrambled PREY) were synthesized by solid-phase peptide synthesis. PREY peptides and scrambled PREY control peptides were conjugated at the C-terminus with biotin-pentylamine by EDC-sulfoNHS coupling (EZ-Link pentylamine-biotin, Fisher Scientific, Rockford, IL). Biotinylated peptides were used to functionalize streptavidin-conjugated paramagnetic particles (Magnesphere, Promega, Madison, WI). For pull-down experiments, mice were sacrificed 4 days after partial carotid ligation surgery. Carotid arteries were removed, immediately frozen in liquid nitrogen, and homogenized on dry ice. Artery homogenate was dissolved in NP40 buffer, and insoluble proteins were separated by centrifugation. Artery protein was incubated with peptide-conjugated beads for 1.5 h. The beads were then washed, and bound proteins were eluted in activated Laemmli sample buffer for further analysis.

Proteomic analysis indicated that several proteins from the vessels with disturbed flow bound to PREY but not by scrambled PREY controls (Table 2). The top candidates identified by proteomic analysis could form a complex and be involved in mechanosensing.[27] We first investigated PREY binding to fibronectin, which is

TABLE 2. Top Five Proteins Identified by Proteomic Analysis

identified proteins	accession no.	molecular weight (kDa)	scrambled abundance	targeted abundance
myosin-11	tr|E9QPE7|E9QPE7	223	0	53
Filamin-A	sp|Q8BTM8|FLNA	281	0	35
vimentin	sp|P20152|VIME	54	0	25
Col6a3	tr|E9PWQ3|E9PWQ3	354	0	24
fibronectin	sp|P11276|FINC	265	0	17

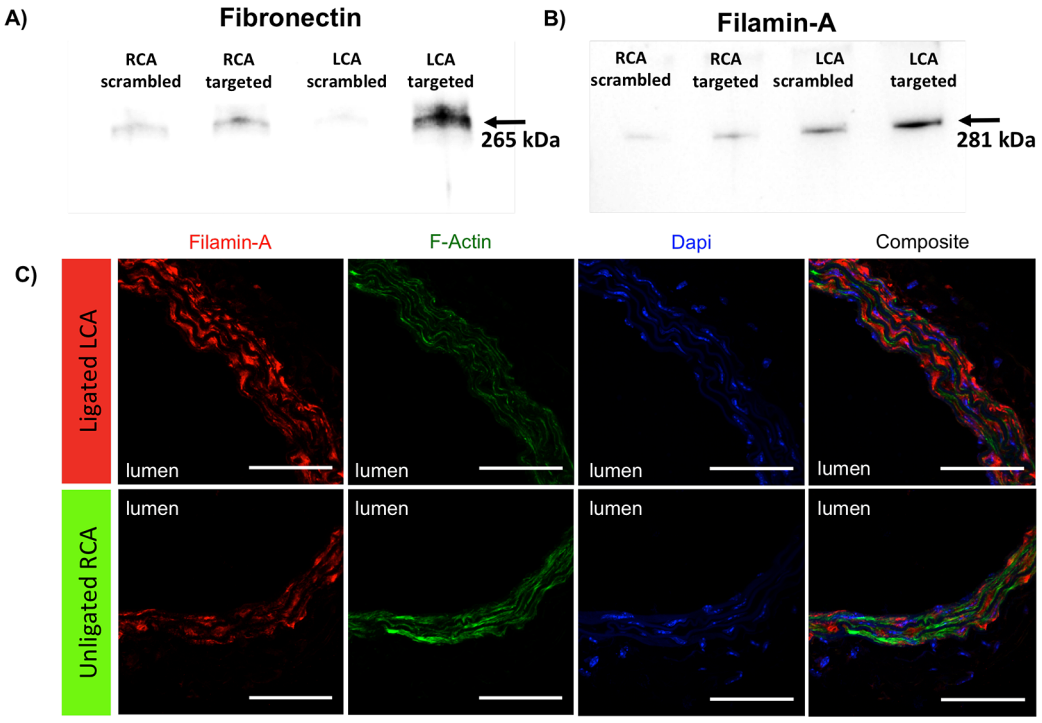

Figure 2. Validation of proteomic analysis. (A) Immunoblot of fibronectin after pull-down with PREY and scrambled PREY. (B) Immunoblot of Filamin-A after pull-down with PREY and scrambled PREY. (C) Immunostaining of Filamin-A in mouse carotid artery sections. Red = Filamin-A, green = F-actin, blue = nucleus. Scale bars are 50 μm.

known to play critical roles in endothelial mechanotransduction and activation. Recent reports have shown that oscillatory shear stress increases fibronectin in the extracellular matrix *in vivo*.[28,29] We also investigated Filamin-A, an actin binding protein involved in cytoskeletal remodeling, regulation of cell migration and cell shape, and anchoring glycoproteins at the cell surface.[30] Filamin-A interacts with caveolin and myoferlin and was chosen for further study due to the homology of the PREY peptide to murine myoferlin.[31,32] In addition, a recent report shows that Filamin-A may be displayed on the cell surface in malignant cells.[33] Microarray studies have shown that Filamin mRNA is increased 2-fold in murine endothelial cells exposed to oscillatory shear compared to laminar shear.[34] In addition, Filamin is recruited to sites where stress is applied to integrins.[35,36]

Increased binding of fibronectin and Filamin-A to PREY-functionalized beads in vessels with disturbed flow was further confirmed by immunoblotting. Pull-downs were performed as described previously, and eluted protein was used for Western blot. Fibronectin was visualized as a single band at 265 kDa (Figure 2A), and Filamin-A was visualized as a single band at 281 kDa (Figure 2B). These results showed the greatest band intensity in both fibronectin and Filamin-A from ligated LCA with targeted peptide, confirming that the PREY peptide pulls down fibronectin and Filamin-A. These data indicate that the PREY peptide may bind to a protein complex involved in mechanotransduction of disturbed shear. In additional experiments, we employed immunofluorescence to visualize Filamin-A in carotid arteries. These confirmed that Filamin-A protein expression is increased in vessels exposed to disturbed flow, and that it is also present on the luminal surface (Figure 2C).

Given the ability to selectively target atheroprone vasculature, nanomedicine offers a promising set of tools for diagnosing, treating, and preventing atherosclerosis.[37] We therefore sought to use the PREY peptide to deliver nanocarriers to atheroprone vasculature. Liposomal nanocarriers were chosen due to their well-documented biocompatibility, ability to carry hydrophilic, hydrophobic, and amphiphilic drugs, and facile

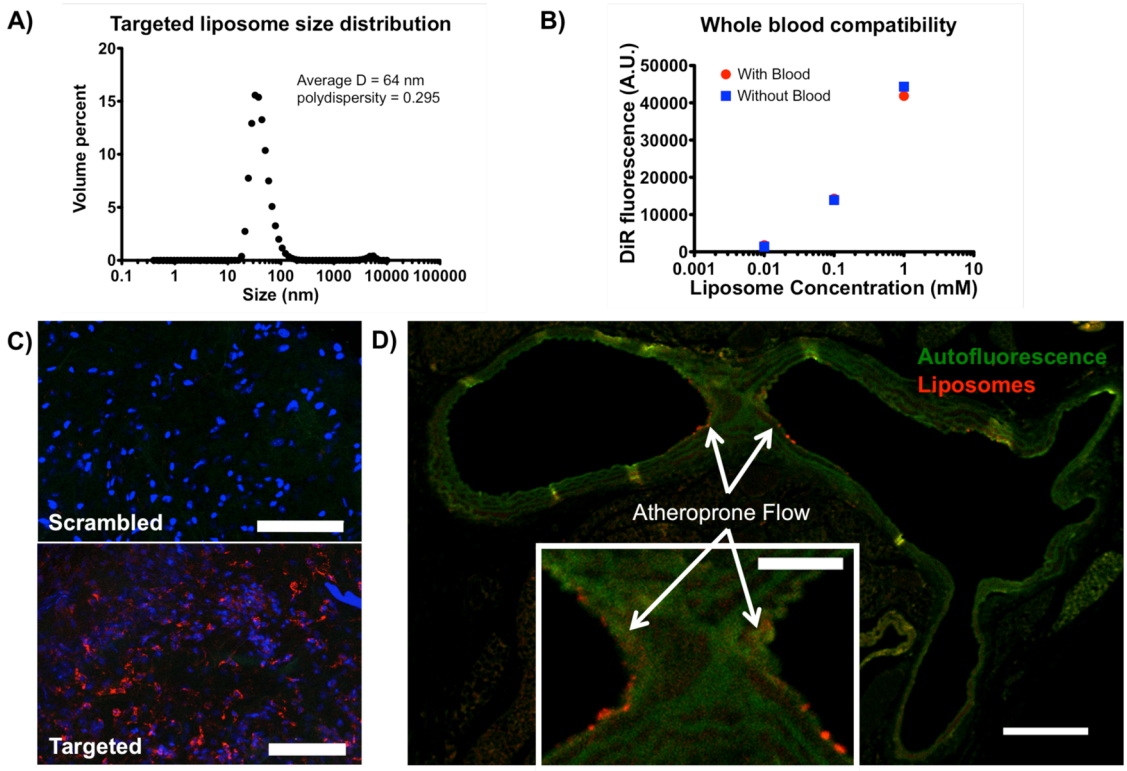

Figure 3. Liposome characterization and vascular targeting. (A) Dynamic light scattering of targeted liposomes. (B) Whole blood compatibility of targeted liposomes. (C) *En face* preparations of ligated left carotid arteries with scrambled and targeted liposome injections. Red = liposome fluorescence, blue = nuclei, green = elastin autofluorescence; scale bars = 100 μm. (D) Cross section of a mouse aortic arch showing targeted liposome accumulation in the lesser curvature of the aortic arch (inset). Green = elastin autofluorescence, red = liposome fluorescence; scale bar = 250 μm, inset scale bar = 100 μm.

chemistry for targeting and extending circulation time.[38] We produced targeted liposomes using the phage-displayed peptide PREY and scrambled PREY. PREY and scrambled PREY were conjugated to 1,2-dipalmitoyl-*sn*-glycero-3-phosphoethanolamine-*N*-(hexanoylamine) (DPHE, Avanti Polar Lipids, Alabaster, AL). Liposomes were formed using a 97.6:2.4 molar ratio of 1,2-dipalmitoyl-*sn*-glycero-3-phosphocholine (DPPC, Avanti Polar Lipids) to peptide−DPHE conjugates, using a thin film rehydration and sonication method.[39,40] 1,1′-Dioctadecyl-3,3,3′,3′-tetramethylindodicarbocyanine perchlorate (DiD) or 1,1′-dioctadecyl-3,3,3′,3′-tetramethylindotricarbocyanine iodide (DiR) was added to the liposome mixture as a fluorescent tracer. DiD-containing liposomes were used for confocal imaging, and DiR-containing liposomes were used for flow cytometry and liposome characterization experiments.

Peptide-targeted liposomes were found to have an average hydrodynamic diameter of 64 nm with a polydispersity of 0.295 by dynamic light scattering (Figure 3A). This size of the liposome was inside the acceptable size range for vascular delivery of nanoparticles.[41] When incubated with whole blood or in buffer, we observed no difference in liposome stability (Figure 3B). These results indicate that targeted liposomes are not destabilized in blood, making them suitable for vascular delivery. The whole blood aggregation assay may not predict the stability of the liposomes in hemodynamic conditions; however, similar liposome compositions have been utilized for vascular delivery. In addition, when injected into mice, liposomes were found to accumulate in the spleen and liver, with negligible accumulation in the heart, lungs, kidneys, and other tissues. This biodistribution is characteristic for clearance of liposomes with similar composition and also indicates a low risk for cardiac or pulmonary toxicity.[42] Liposome solutions (0.9 mg of fluorophore per kg body weight, 1.6 mM lipids in Hanks buffered saline (HBS)) were administered to mice by intravenous injection through the tail vein 4 days after the partial ligation procedure. Fifteen hours post-injection, mice were euthanized, and arteries were analyzed for liposome targeting. Liposome uptake was compared between LCA and RCA using scrambled PREY-conjugated liposomes as a control.

Figure 3C shows *en face* preparations of ligated left carotid arteries after liposome injection. We found that PREY-targeted liposomes accumulate in the partially ligated LCA (Figure 3C, bottom) while scrambled PREY-conjugated liposomes showed minimal uptake in the ligated vessel (Figure 3C, top). We also investigated uptake of targeted nanoparticles in the lesser curvature of the aortic arch, another vascular location known to have disturbed flow.[1] Figure 3D shows a cross

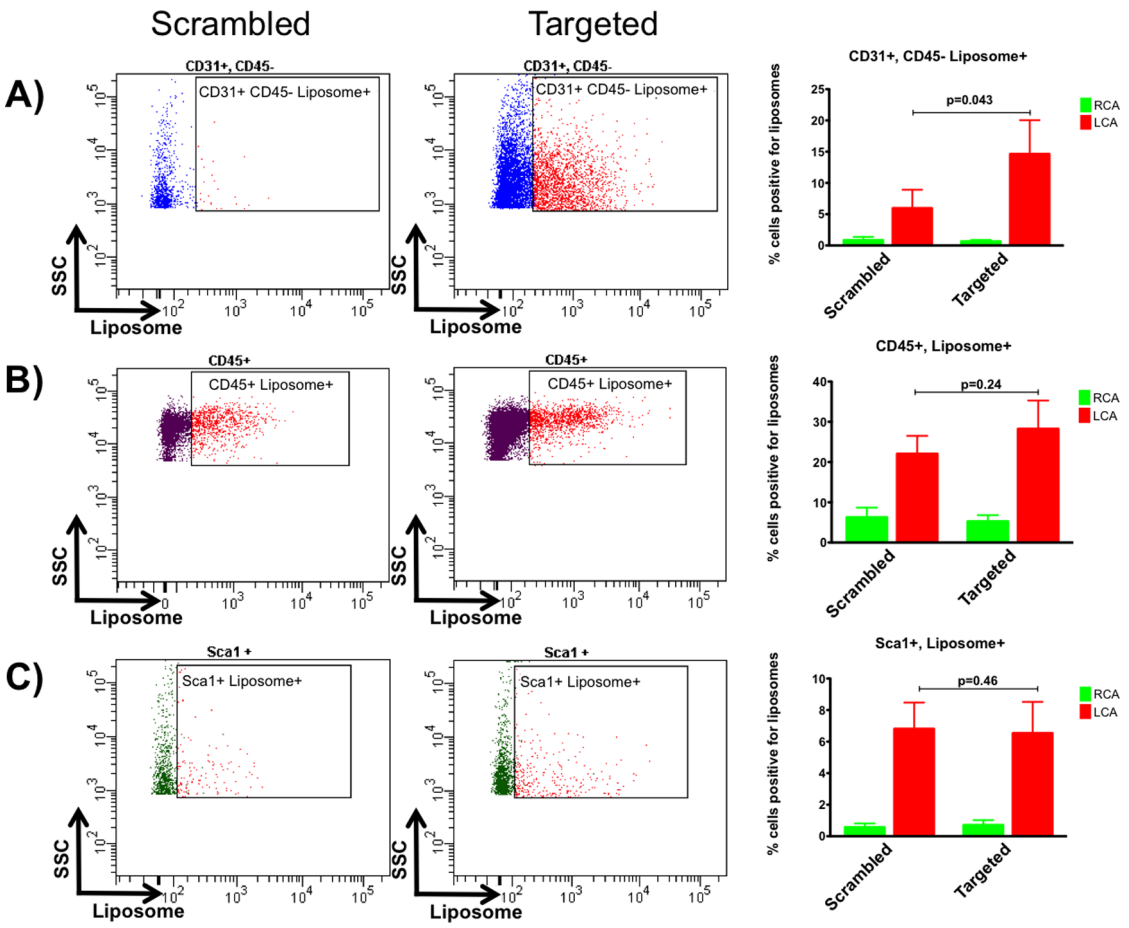

Figure 4. Flow cytometry analysis of cellular targeting. (A) CD31$^+$ and CD45$^-$ cell population; (B) CD45$^+$ cell population; (C) Sca1$^+$ cell population.

section of the aortic arch of a mouse after liposome injection. We observed accumulation of PREY-targeted liposomes in the lumen at the inner curvature of the aortic arch in mice without partial carotid ligation surgery. These results demonstrate that PREY-targeted liposomes home to natural regions of disturbed flow *in vivo*.

Next we sought to determine the vascular cell type targeted by PREY liposomes. To do this, we performed flow cytometry on arteries after liposome injection. Single cell suspensions from the LCA and RCA were co-stained with platelet endothelial cell adhesion molecule (CD31) as a marker for endothelial cells, protein tyrosine phosphatase receptor type C (CD45) as a marker for all leukocytes, and stem cell antigen-1 (Sca1) as a marker for stem cells which are known to reside in the vascular adventitia.[43] Dead cells and cell clusters were excluded from analysis. This analysis showed that PREY-targeted liposomes accumulate in CD31$^+$ endothelial cells significantly more than scrambled PREY-conjugated liposomes (Figure 4A). Increased uptake of liposomes in the left carotid artery was also observed in CD45$^+$ and Sca1$^+$ cells; however, no significant difference was observed between PREY and scrambled PREY liposomes (Figure 4B,C). This is likely due to uptake of liposomes by immune cells, including monocyte/macrophages, which are known to accumulate in vasculature with activated endothelium. Increased numbers of positive leukocytes in the ligated artery with both PREY and scrambled PREY liposomes could reflect recruitment of these cells from circulation by the activated endothelium.

We next sought to determine if PREY-targeted nanoparticles could be used for drug delivery to improve endothelial function in atheroprone areas under disturbed flow. Oxidative stress is a major cause of endothelial dysfunction in diseases such as atherosclerosis, hypertension, and diabetes.[5,44] Previously, we have shown that a major source of reactive oxygen species (ROS) in endothelial cells exposed to disturbed flow is uncoupled nitric oxide synthase.[45] Tetrahydrobiopterin (BH_4) is a critical cofactor for the NO synthases. BH_4 permits transfer of electrons from the prosthetic heme group to the guanidino nitrogens of L-arginine, allowing formation of NO. In the absence of BH_4, electrons from the NOS heme group reduce oxygen to produce superoxide. We have found that laminar shear induces the synthesis of BH_4, while it is deficient in endothelial cells exposed to oscillatory shear stress.[8,46] BH_4 oxidation to inactive BH_2 also

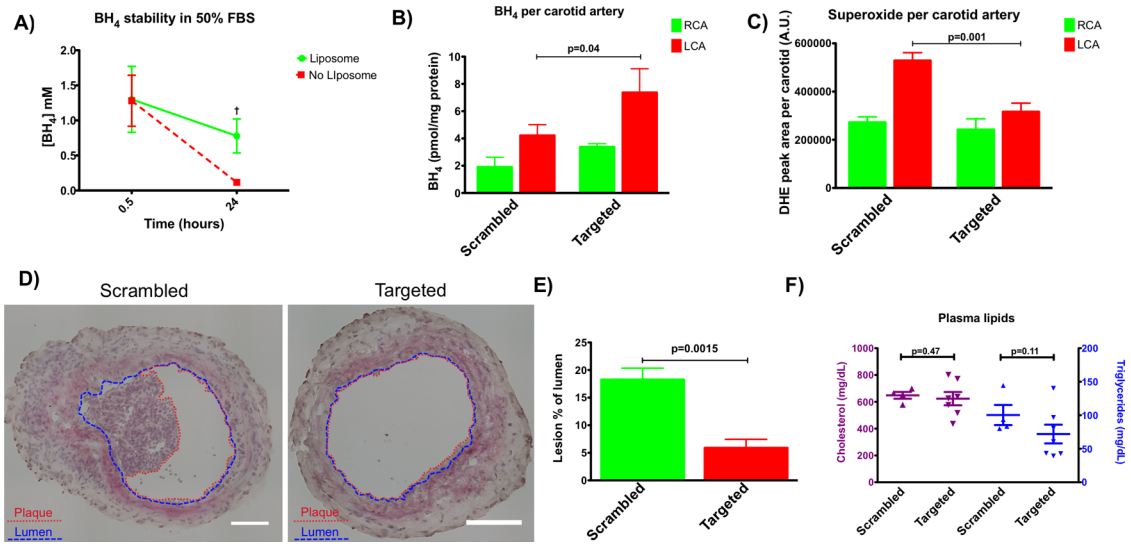

Figure 5. Liposomal delivery of tetrahydrobiopterin. (A) Liposomes maintained the stability of BH_4 in serum significantly more than unencapsulated BH_4 after 24 h; $p = 0.017$. (B) Liposome delivery significantly increased BH_4 concentration in the ligated artery with targeted liposomes but not with scrambled controls; $p = 0.040$. (C) Liposomal delivery of BH_4 significantly decreased superoxide concentration in the ligated artery with targeted liposomes but not with scrambled controls; $p = 0.001$. (D) Liposomal delivery of BH_4 significantly reduced plaque burden in the ligated left carotid artery of $ApoE^{-/-}$ mice fed a high fat diet for 7 days. Plaque is outlined in red, and lumen is outlined in blue. Scale bars = 100 μm. (E) Plaque area quantified; $p = 0.0015$. (F) Liposome delivery did not change lipid metabolism as measured by total serum cholesterol and triglycerides; $p = 0.47$ and 0.11, respectively.

occurs in endothelial cells exposed to disturbed flow and further depletes intracellular BH_4. In the partial carotid ligation model, we have confirmed that BH_4 levels are reduced, and that oral supplementation of BH_4 can recouple NOS and abrogate the accelerated atherosclerosis that occurs in the ligated artery.[45,47,48] Challenges associated with delivery of exogenous BH_4 include oxidation and poor cellular uptake in endothelial and parenchymal cells.[49] We therefore sought to use the PREY-targeted liposomal nanocarriers to protect BH_4 from oxidation in circulation and deliver BH_4 to endothelial cells in atheroprone regions.

BH_4 was encapsulated in liposomes by a thin film rehydration technique.[50] We found that liposome-encapsulated BH_4 was significantly more stable than free BH_4 over 24 h incubation in 50% serum (Figure 5A). To determine if targeted nanoparticles could increase BH_4 concentration in target tissue, targeted nanoparticles containing BH_4 were injected by tail vein 1 day post-ligation in wild-type mice, and the carotids were removed for measurement of pterins 7 days later. PREY-targeted nanoparticles were found to significantly increase BH_4 concentration in target tissue compared to scrambled PREY controls (Figure 5B). Next, we measured superoxide levels in carotid arteries by monitoring the conversion of dihydroethidium (DHE) to its superoxide adduct, 2-hydroxyethidium. PREY-targeted liposome delivery of BH_4 significantly decreased superoxide in the ligated artery compared to scrambled peptide controls (Figure 5C). These results indicate that targeted delivery of BH_4 can successfully increase the availability of this critical cofactor and effectively rescue endothelial dysfunction as indicated by the reduced production of superoxide.

To determine if targeted BH_4 delivery can prevent plaque formation in response to disturbed shear stress and hypercholesterolemia, apolipoprotein (Apo) E deficient mice underwent partial carotid artery ligation surgery and were fat fed to induce atherosclerosis.[51,52] This model leads to accelerated atherosclerotic lesions after 1 week of a high-fat diet.[9] Mice received nanoparticle injections at 1 day post-ligation, and end point experiments were conducted at 7 days post-ligation. We found a significant decrease in plaque burden in the ligated left carotid artery of mice that received PREY-targeted liposome injections compared to scrambled controls (Figure 5D,E). BH_4-containing targeted liposomes did not significantly alter total cholesterol or triglycerides in these animals (Figure 5F). This indicates that nanocarrier delivery of BH_4 prevents atherosclerosis caused by endothelial dysfunction in areas of disturbed flow, even in the case of hypercholesterolemia.

CONCLUSION

Atherosclerotic lesions develop when focal endothelial dysfunction caused by disturbed shear stress is compounded by systemic risk factors such as hypercholesterolemia. Targeted drug delivery to areas of disturbed flow is a promising approach to prevent atherosclerosis before lesions develop. Because prediction of these atheroprone areas is impossible, programming nanocarrier functions to navigate to and detect atheroprone areas is an ideal but unmet need.

To accomplish this, we first developed a method to target atheroprone vasculature by *in vivo* phage display. We discovered four peptides that selectively target atheroprone vasculature. A candidate peptide, PREY, was used to form targeted liposomal nanocarriers, which were observed to accumulate in areas of disturbed shear *in vivo*. We also showed that the PREY-targeted liposomes home to endothelial cells in atheroprone vasculature, making this nanocarrier a promising candidate to treat endothelial dysfunction. To improve endothelial function caused by disturbed shear stress, we targeted uncoupled nitric oxide synthase by delivering BH_4 as a candidate drug. PREY-targeted liposomes were shown to overcome known delivery barriers for BH_4 by stabilizing BH_4 in serum and delivering BH_4 to target tissue. BH_4 delivery was shown to reduce vascular superoxide in the ligated artery of C57/BL6J mice and reduce plaque formation in the ligated artery of $ApoE^{-/-}$ mice. Our results indicate that PREY-targeted nanocarrier delivery of BH_4 could be used as a prophylactic treatment for atherosclerosis. In addition to allowing nanoparticle drug delivery, peptides like PREY may be useful for diagnostic imaging to assess residual risk factors such as the number and location of areas of atheroprone vasculature.

MATERIALS AND METHODS

Unless otherwise noted, all reagents were purchased from Sigma-Aldrich, St. Louis, MO.

Animals Studied. Wild-type C57BL/6 and $ApoE^{-/-}$ mice were purchased from Jackson Laboratories (Bar Harbor, ME). The institutional animal care and use committee at Vanderbilt University approved all animal protocols. All *in vivo* experiments were performed in a partial carotid artery ligation model of disturbed flow.[9] Male mice at an age of 10−14 weeks underwent a surgical procedure in which the LCA was exposed and three of four of its branches—the left external carotid, left internal carotid, and the occipital artery—were ligated with 6-0 silk suture, while the superior thyroid artery was left intact. Care was taken to avoid damaging the superior thyroid artery during ligation. During the same surgical operation, the RCA was surgically exposed and manipulated in the same way as the LCA but not ligated. The RCA served as a sham control. Doppler ultrasound was performed using a VisualSonics Vevo 770 (Fujifilm VisualSonics, Inc., Toronto, Canada) microimaging system to visualize blood flow in the ligated and unligated arteries. Images were acquired using the RMV-704 ultrasound probe transmitting at 100% power at a frequency of 30 MHz with a receiving Doppler gain of 10 dB.

***In Vivo* Phage Display.** *In vivo* phage display was performed in C57/BL6 mice 4 days post-ligation. Two peptide libraries were screened in this study, the Ph.D.-12 and Ph.D.-C7C libraries (New England Biolabs, Ipswich, MA, Cat# E8110S and E8120S, respectively). Phage peptide libraries were injected into the tail vein of the mice at a concentration of 2×10^{11} plaque-forming units to ensure a 100-fold representation of all clones in the phage library containing a theoretical 2×10^9 different clones. After 2.5 h of circulation time, mice were euthanized by CO_2 asphyxiation and perfused at physiological pressure with normal saline containing 10 U·mL^{-1} heparin, and then both carotid arteries were surgically removed and processed separately. In order to remove unbound phages, the excised arteries were cannulated with a 30 gauge syringe and washed with 0.5 mL Tris-buffered saline (TBS) with 0.1% v/v Tween-20 (TBST) and transferred to fresh TBST. In order to expose the endothelium for the next steps, each artery was cut lengthwise with a number 10 scalpel. Arteries were then washed with nonspecific elution buffer consisting of 0.1 M glycine/HCl (pH 2.2) with 1 mg·mL^{-1} bovine serum albumin to remove phages bound to the surface of the vessels and weakly bound phages. Next, phages were eluted with 100 mM triethanolamie in TBS.[17] The eluted phages were then used to transform *Escherichia coli* for amplification, and the number of phages binding to the target condition was quantified by titration according to the manufacturer's protocol. For amplification, *E. coli* were transformed at early log phase (OD_{600} 0.01−0.06) with phages and cultured for 4.5 h with vigorous shaking. Phages were then purified by ultracentrifugation and overnight precipitation into 20% w/v polyethylene glycol (MW = 8000) with 2.5 M NaCl. Amplified phages from the LCA were then used in the subsequent rounds of phage display following the same procedures.

LB agar plates for titration contained 0.2 mM isopropyl-β-D-thiogalactoside, 0.1 mM 5-bromo-4-chloro-3-indolyl-β-D-galactoside, 10 g·L^{-1} bacto-tryptone, 5 g·L^{-1} yeast extract, 10 g·L^{-1} NaCl, and 15 g·L^{-1} agar. Visualizing β-gal-positive colonies allowed for quantification of phage titer. After the third and fourth round of phage panning, 10 colonies were sequenced from titration plates to identify consensus sequences. For sequencing, colonies were picked using sterile pipet tips and deposited into 30 μL of platinum PCR Supermix (Invitrogen, Grand Island, NY, Cat# 11306-016) containing 0.5 μM forward and reverse primers (forward primer 5′-GTCATTGTCGGCGCA-ACTATCGG-3′, reverse primer 5′-CCCTCATAGTTAGCGTAACG-3′). Amplified DNA fragments were purified using QIAquick PCR spin columns (Qiagen, Hilden, Germany, Cat# 28104) and diluted in DNase-free water for sequencing. Sanger sequencing was performed at the Vanderbilt Technologies for Advanced Genomics using the reverse primer from PCR amplification.[53]

To validate the affinity of consensus sequences, consensus clones were amplified as described previously by inoculating an *E. coli* culture with a consensus clone colony and injected following the same procedures as *in vivo* phage library panning. Titration of phages binding to the LCA *versus* RCA was used to determine the relative affinity for the target condition. The titer of phages recovered was normalized to the protein content of the corresponding vessel. For measurement of protein concentration, carotid artery segments were placed in 50 μL of RIPA lysis buffer (Thermo Scientific, Rockford, IL, Cat# 89900) containing protease and phosphatase inhibitors (Roche, Indianapolis, IN, Cat# 05892970001 and 04906845001, respectively) and sonicated for 1 min on ice to release protein. Protein content was measured by small-volume BCA assay (Thermo Scientific, Cat# 23225).

Peptide Synthesis. Peptides were synthesized on a PS3 three-channel serial peptide synthesizer (Protein Technologies, Inc., Tucson, AZ) on low-substitution glycine-loaded Wang or 2-chlorotrityl resin support using standard solid-phase fluorenylmethyloxycarbonyl chloride chemistry. *N*-Methylpyrrolidone (Fischer Scientific) was utilized as a solvent in all peptide syntheses. *O*-(6-Chlorobenzotriazol-1-yl)-*N*,*N*,*N*′,*N*′-tetramethyluronium hexafluorophosphate was used as an activator (Chempep, Wellington, FL) in the presence of *N*-methylmorpholine. All amino acids were double coupled in order to maximize yield and purity. All peptides were N-acetylated by reaction with acetic anhydride. Peptides were cleaved and deprotected in trifluoroacetic acid/water/triisopropylsilane (95/2.5/2.5). Successful peptide synthesis was verified through electrospray ionization mass spectrometry (ESI-MS) analysis on a Waters Synapt ESI-MS. The peptide was then further purified by reverse-phase high-performance liquid chromatography (HPLC) on a Waters 1525 binary HPLC pump outfitted with an extended flow kit, a Waters 2489 UV/visible detector, and a Phenomenex Luna C-18(2) AXIA packed column (100A, 250 × 21.2 mm, 5 μm).

HPLC-grade water with 0.05% formic acid (solvent A) and HPLC-grade methanol with 0.05% formic acid (solvent B) were used as the mobile phases, and the peptide was purified utilizing a 90% A to 90% B gradient over 25 min at a flow rate of 16 mL·min^{-1}. Methanol was removed from purified fractions with a rotary evaporator, and the purified fractions were then frozen and lyophilized. Peptide purity was verified through ESI-MS.

Determining a Potential Binding Partner for the PREY Peptide. To determine the binding partner for the PREY peptide, we performed a pull-down followed by proteomics analysis. PREY peptides and scrambled PREY control peptides were conjugated at the C-terminus with biotin-pentylamine by EDC-sulfoNHS coupling (EZ-Link pentylamine-biotin, Fisher Scientific, Rockford, IL). Conjugates were purified by dialysis overnight to remove excess pentylamine-biotin. Conjugation products were confirmed by ESI-MS. Two milligrams of each peptide−biotin conjugate was mixed with 1 mg of streptavidin-conjugated paramagnetic particles (Magnesphere, Promega, Madison, WI). To remove excess peptide, beads were washed five times prior to use. For pull-down experiments, mice were sacrificed 4 days after partial carotid ligation surgery. Carotid arteries were removed, immediately frozen in liquid nitrogen, and homogenized on dry ice. Artery homogentate was dissolved in 800 μL of NP40 buffer (0.5% Triton-100 in Tris-buffered saline pH = 7.8 with protease inhibitors), and insoluble proteins were cleared by centrifugation. Four hundred microliters of protein was mixed with 100 μg of peptide-conjugated beads and incubated for 1.5 h at room temperature. Beads were washed four times with NP40 buffer, and proteins were eluted with 30 μL of 1× activated Laemmli buffer by heating to 70 °C for 10 min.

Shotgun proteomic analysis of eluate was performed by first resolving eluted proteins approximately 1 cm using a 10% Novex precast gel and then performing in-gel tryptic digestion to recover peptides.

Resulting peptides were analyzed by a 70 min data-dependent LC-MS/MS analysis. Briefly, peptides were autosampled onto a 200 mm × 0.1 mm (Jupiter 3 μm, 300A) self-packed analytical column coupled directly to an LTQ (ThermoFisher) using a nanoelectrospray source and resolved using an aqueous to organic gradient. A series of full-scan mass spectra followed by five data-dependent tandem mass spectra (MS/MS) were collected throughout the run, and dynamic exclusion was enabled to minimize acquisition of redundant spectra. MS/MS spectra were searched *via* SEQUEST against a mouse database that also contained a reversed version for each of the entries (http://www.ncbi.nlm.nih.gov/pubmed/7741214). Identifications were filtered and collated into spectral count numbers at the protein level using Scaffold (Proteome Software).

Western Blot. Filamin-A and fibronectin pull-down was confirmed by Western blot. Pull-downs were performed as described previously, and eluted protein was used for Western blot. Proteins were run on a 4−20% SDS-PAGE gel and transferred to polyvinylidene fluoride membranes overnight at 30 V at 4 °C. Membranes were blocked for 1 h in 5% milk in 0.1% TBST. Anti-Filamin-A antibody (ab51217, Abcam, Cambridge, MA) and anti-fibronectin antibody (ab23750, Abcam) were diluted 1:500 in TBST and incubated with the membranes for 1 h at room temperature. Filamin-A was visualized as a single band at 281 kDa in Western blots. Fibronectin was visualized as a single band at 265 kDa.

Immunostaining. Immunofluorescence staining was performed on fix-perfused mouse carotid arteries embedded in optimal cutting temperature (OCT). Five micron sections were sliced in a serial sequence. Samples were permeabilized with 0.1% Triton X-100 (Sigma-Aldrich). Antigen blocking was performed with 5% bovine serum albumin (BSA) prior to incubation with anti Filamin-A antibody (ab51217, Abcam). Additional blocking with 10% donkey serum was performed before incubation with secondary antibodies. Donkey polyclonal antibodies conjugated to Alexa Fluor 488, 555, or 647 were used for binding primary antibodies. Where applicable, samples where then subsequently incubated with phalloidin−Alexa 488 (Life Technologies) for visualization of F-actin. 4',6-Diamidino-2-phenylindole (Invitrogen) was added in the last wash following incubation with secondary antibodies or phalloidin. All slides were mounted with Prolong Antifade media (Life Technologies).

Targeted Liposome Synthesis and Characterization. The phage-displayed peptide acetyl-GSPREYTSYMPHGSGS-COOH (AcPREY) and the scrambled control peptide acetyl-THRPMSSYEPGYGSGS-COOH (AcPREYs) were conjugated to DPHE (Avanti Polar Lipids, Alabaster, AL, Cat# 870125C) to form targeted liposomes by anhydrous *N*-hydroxyuccinimide (NHS) and *N*,*N*′-dicyclohexylcarbodiimide (DCC) reaction. Two equivalents of the acetylated peptide was added to 4 equiv of DCC and NHS and mixed with 1 equiv of DPHE dissolved in a 1:1 mixture of anhydrous dimethylformamide (DMF) and anhydrous methanol under nitrogen at room temperature. Two equivalents of triethylamine in DMF was added to the reaction to act as a catalyst. The reaction was allowed to proceed overnight; however, robust precipitation of dicyclohexylurea was observed after 30 min. The reaction product was filtered through a 0.45 μm PTFE filter to remove insoluble products, precipitated twice into cold diethyl ether, and dried *in vacuo*. Reaction products were then dissolved in a 65/35/8 mixture of chloroform/methanol/water, diluted into water, and purified by flash chromatography over disposable octadecyl C_{18} columns (Bakerbond spe, Avantor Performance Materials, Center Valley, PA, Cat# 720-06). Purified AcPREY-DPHE product was eluted with 100% methanol, precipitated into cold diethyl ether, and dried *in vacuo*. Reaction products were confirmed by ESI-MS.

Liposomes were formed using a 97.6:2.4 molar ratio of DPPC (Avanti Polar Lipids, Cat# 850355C) and AcPeptide−DPHE conjugates. DiD or DiR was added to the liposome mixture as a fluorescent tracer. To form liposomes, 2.08 μmol of DPPC (25 mg·mL^{-1} in chloroform), 0.052 μmol of AcPeptide−DPHE (12.5 mg·mL^{-1} in methanol), and either 0.15 μmol of DiD (25 mg·mL^{-1} in methanol) or 0.14 μmol of DiR (25 mg·mL^{-1} in methanol) were combined mixed well in a 13 × 100 mm glass test tube and dried under nitrogen and subsequently *in vacuo* for at least 2 h. The mixture was resuspended in 1.3 mL of HBS solution containing 100 mM NaCl, 20 mM HEPES/NaOH pH 7.5, and 0.02% w/v sodium azide and sonicated for 1.5 h to yield a 1.6 mM liposome solution containing 0.12 mM DiD or DiR. DiD-containing liposomes were used for confocal imaging, and DiR-containing liposomes were used for flow cytometry, IVIS imaging, and liposome characterization experiments.

The hydrodynamic diameter was characterized on a Malvern Zetasizer Nano-ZS (Malvern Instruments Ltd., Worcestershire, UK).

Whole Blood Compatibility. Whole blood compatibility of the liposomes was determined by performing a whole blood aggregation assay as previously described.[54] Targeted liposomes were formed as previously described at 1.6 mM concentration in HBS. Serial dilutions of the liposomes were then added to human whole blood at a final liposome concentration of 1, 0.1, and 0.01 mM. As a control, the micelles were also added to HBS at the same concentration. Blood−liposome mixtures were placed on a shaker for 5 min and incubated at 37 °C for an hour. The plates were then centrifuged at 500*g* for 5 min. One hundred microliters of supernatant from each well was transferred to a black clear-bottom 96-well plate, and DiR fluorescence was measured with an excitation of λ = 750 nm and an emission wavelength of λ = 780 nm on a TECAN Infinite M1000 Pro plate reader (Tecan Group Ltd., Mannedorf, Switzerland).

Tetrahydrobiopterin Encapsulation and Protection from Oxidation. BH_4 was encapsulated in liposomes by a thin film rehydration technique.[50] First, lipids in organic solvent were dried as previously described. Immediately before formation of liposomes, BH_4 was dissolved in HBS at 17 mM. Lipids were then reconstituted in 17 mM BH_4 in HBS and sonicated for 1.5 h to form liposomes. BH_4-containing liposomes were found to have the same hydrodynamic diameter as liposomes prepared without BH_4. Because BH_4 is known to rapidly oxidize in physiological conditions, the ability of the liposomes to protect BH_4 from oxidation was examined. Liposomes formed with BH_4 were incubated at 1.7 mM in 50% FBS in HBS. Samples were collected at 30 min and 24 h to determine the amount of BH_4 remaining in solution.

Liposome Injections. For liposome localization and targeting experiments, liposome solutions were administered to mice by

intravenous injection through the tail vein 4 days after partial carotid ligation at a concentration of 0.9 mg of fluorophore per kg body weight. Fifteen hours post-injection, mice were euthanized by CO_2 inhalation and perfused with heparinized saline as described previously. Arteries were then analyzed for liposome uptake by flow cytometry, IVIS imaging, and confocal microscopy. Liposome uptake was compared between LCA and RCA using scrambled peptide-targeted liposomes as a control.

Flow Cytometry. To obtain single cell suspension solutions from sample arteries, carotid arteries were surgically removed and placed into a digestion solution consisting of phenol-red-free RPMI 1640 medium (Life Technologies, Grand Island, NY) with L-glutamine, 10% fetal bovine serum, 1 mg·mL^{-1} collagenase A, 1 mg·mL^{-1} collagenase B, and 0.1 mg·mL^{-1} DNase 1 (Roche Diagnostics, Indianapolis, IN, Cat# 10103578001, 11088807001, and 10104159001, respectively). The arteries were minced with sharp scissors for 2 min and then placed on a shaker for 30 min at 37 °C. Next, the arteries were filtered using a 70 μm cell strainer to obtain cell suspensions. The cell strainer was washed three times with 10 mL of RPMI 1640 to recover dissociated cells. Next, the cells were centrifuged at 300*g* for 10 min and then transferred to FACS tubes for the rest of processing. All subsequent steps took place in FACS buffer consisting of 1× PBS with Ca^{2+} and Mg^{2+}, 1% bovine serum albumin, and 0.1% sodium azide. The cell samples were first processed by blocking Fc receptors with anti-CD16/CD32 for 10 min at 4 °C (BDbiosciences, clone 2.4G2, Cat# 553142) for 10 min on ice. The cells were centrifuged at 300*g* for 5 min and washed once with 1 mL of FACS buffer. Cell populations were characterized by Brilliant Violet 510 (BV510)-conjugated anti-CD45 antibody (BioLegend, clone 30-F11, Cat# 103137), phycoerythrin-conjugated anti-CD31 antibody (BD pharmingen, clone MEC13.3, Cat# 561073), and fluorescein isothiocyanate-conjugated anti-Ly-6A/E (Sca1) antibody (BD Pharmingen, clone E13-161.7, Cat# 553335). CD31 was considered a marker for endothelial cells, CD45 as a marker for all leukocytes, and Sca1 as a marker for stem cells.[43] Cells were incubated with staining solutions for 30 min at 4 °C and then washed twice with FACS buffer. For dead cell staining, 7-aminoactinomycin-D (7-AAD) (eBioscience, Cat# 00-6993-50) was added to cells 10 min prior to sorting. Acquisition of a minimum of 500 000 events was on a BD FACS Canto II system (8-color, blue, red, violet, Cat# 338962), and analysis was performed on BD FACSDiva software version 6.1.3 (BD Biosciences).

Gating was applied based on the single stain and flow minus one controls. Dead cells and cell clumps were excluded by gating on 7-AAD and then for single cells based on forward scatter area *versus* forward scatter height.

Confocal Microscopy. For confocal microscopy experiments, liposomes were formulated with DiD. For all imaging experiments, mice were euthanized by CO_2 inhalation 15 h post-injection and perfused with heparinized saline as described previously. For aortic arch samples, mice were subsequently perfused at physiological pressure with 10% neutral buffered formalin for 5 min and then dissected to isolate a tissue block containing the heart, lungs, and whole aorta. Tissue blocks were further fixed in 10% buffered formalin for 24 h and subsequently paraffin-embedded and sectioned at 5 μm. The Vanderbilt Translational Pathology Shared Resource performed all embedding and sectioning. For carotid artery samples, the carotid arteries were surgically isolated, cannulated with a 30 gauge syringe, and washed with TBST. Next, arteries were cut longitudinally to expose the endothelium and mounted on microscope slides with 4% paraformaldehyde in PBS without Ca^{2+} and Mg^{2+}. Carotid artery samples were counterstained with Hoechst to visualize nuclei. Fluorescence images were acquired using a Zeiss 710 confocal laser microscope.

Nanoparticle Delivery of BH_4. Liposomes containing BH_4 were administered 1 day post-ligation by tail vein injection at 0.9 mg of fluorophore per kg body weight. Animals studied included apolipoprotein E knockout (ApoE$^{-/-}$) and C57/BL6J mice. Seven days post-ligation, animals were sacrificed and end point analysis was performed.

Quantification of BH_4. BH_4 concentrations were measured by HPLC as previously described.[45,55] To analyze arterial levels of BH_4, 7 days post-ligation, mice were sacrificed by CO_2 inhalation and perfused with ice-cold heparinized PBS. Carotid arteries were surgically isolated, and care was taken not to stretch or damage the arteries. Carotid arteries were then snap frozen in liquid nitrogen. To obtain artery homogenate, carotid arteries were ground using a mortar and pestle precooled on dry ice. Artery homogenate was then dissolved in 110 μL of lysis buffer (50 mM Tris-HCl, pH 7.4, 1 mM dithiothreitol, and 1 mM ethylenediaminetetraacetic acid), and 12.5 μL of a 1:1 mixture of 1.5 M $HClO_4$ with 2 M H_3PO_4 was added to precipitate proteins. Samples were then centrifuged at 13 500*g* for 2 min at 4 °C. Next, differential oxidation was performed in acid and alkaline preparations. BH_4 was detected by fluorescence (ex = 350 nm, em = 450 nm) at a retention time of 9.5 min using a 5 × 250 mm × 5 um C-18 column that was used with an isocratic solvent system consisting of 95% water with 5% methanol at a flow rate of 1 mL·min^{-1}. Concentrations were normalized to protein content as measured by BCA assay according to the manufacturer's protocol.

Measurement of Superoxide. To evaluate the effect of nanoparticle treatment on vascular ROS production, 2-hydroxyethidium formation from DHE was measured by HPLC as previously described.[56] To measure arterial superoxide, 7 days post-ligation, mice were sacrificed by CO_2 inhalation and perfused with ice-cold Krebs−HEPES buffer containing 99 mM NaCl, 4.69 mM KCl, 25 mM $NaHCO_3$, 1.03 mM KH_2PO_4, 5.6 mM D(+)-glucose, 20 mM Na-HEPES, 2.5 mM $CaCl_2 \times 2H_2O$, and 1.2 mM $MgSO_4 \times 7H_2O$. Carotid arteries were surgically isolated, and care was taken not to stretch or damage the arteries. Each carotid artery was placed on 1 mL of ice-cold Krebs−HEPES buffer and carefully trimmed to remove adventitial fat. Each artery was then cut into five equally sized rings. A 5 μM stock solution of DHE in anhydrous dimethylsulfoxide (DMSO) was created by degassing DMSO under nitrogen for 30 min and adding to fresh DHE. Five microliters of this stock solution was added to each artery, and the samples were incubated in the dark at 37 °C for 30 min. Next, the artery rings were placed in 300 μL of ice-cold methanol and homogenized using a dounce homogenizer. Samples were then filtered through 0.2 μm PTFE filters and stored at −80 °C in the dark until running. 2-Hydroxyethidium was detected by fluorescence (ex = 480 nm, em = 580 nm) at a retention time of 13.5 min using a 4.5 × 250 mm reverse-phase C-18 column (Nucleosil, Sigma-Aldrich, St. Louis, MO) and a mobile phase of 60% acetonitrile with 0.1% trifluoroacetic acid with a linear increase in acetonitrile concentration from 37 to 47% over 23 min at a flow rate of 0.5 mL·min^{-1}.

Quantification of Plaque Burden in ApoE$^{-/-}$ Mice. ApoE$^{-/-}$ mice received the partial carotid artery ligation surgery and were immediately fed a western diet (Teklad #88137, 42% from fat, Harlan Laboratories, Indianapolis, IN). Seven days post-ligation, mice were sacrificed by CO_2 inhalation.[52] Mice were then perfused with ice-cold heparinized saline and then perfused at physiological pressure with 10% neutral buffered formalin. Next, carotid arteries were surgically removed, cleaned of excess adventitial fat, and mounted in OCT mounting medium (TissueTek, VWR, Radnor, PA). Cryosections were obtained at 5 μm thickness. Sections were stained with hematoxylin and eosin. To quantify plaque burden, lumen area was traced and plaque area expressed as a percentage of the total lumen area. Average lumen area covered was calculated for $N = 4$ animals per group.

Serum Lipid Analyses. The serum total cholesterol and triglyceride levels were determined in serum samples using enzymatic assays (Roche). Fast-performance liquid chromatography was performed on an HPLC system model 600 (Waters, Milford, MA) using a Superose 6 column (Pharmacia, Piscataway, NJ) in both groups of samples ($n = 4$ and $n = 4$).

Statistical Analysis. Phage clone binding was evaluated based on a two-tailed Wilcoxan matched-pairs signed rank test. Targeted liposome injections were compared to scrambled controls using Student's *t* test.

Conflict of Interest: The authors declare no competing financial interest.

Acknowledgment. This work was supported by American Heart Association Pre-Doctoral Fellowship 13PRE14730011,

National Science Foundation (NSF) CAREER CBET 1056046 and, National Institutes of Health (NIH) Grants UH2 TR000491, R01HL039006, P01HL058000, P01GM015431, R01HL108701, and R01HL105294. Confocal imaging was performed in part through the use of the VUMC Cell Imaging Shared Resource (supported by NIH Grants CA68485, DK20593, DK58404, HD15052, DK59637, and Ey008126). Dynamic light scattering and TEM were conducted at the Vanderbilt Institute of Nanoscale Science and Engineering, using facilities renovated under NSF Grant ARI-R2 DMR-0963361. Histological sectioning was performed in part by the Vanderbilt Translational Pathology Shared Resource (TPSR). The Proteomics Core of the Vanderbilt Mass Spectrometry Resource Center performed proteomic analysis. A.E.N. performed Western blots. K.R.C.M. performed immunostaining. S.H.L. performed phage sequencing and confocal microscopy.

REFERENCES AND NOTES

1. Ku, D. N.; Giddens, D. P.; Zarins, C. K.; Glagov, S. Pulsatile Flow and Atherosclerosis in the Human Carotid Bifurcation. Positive Correlation between Plaque Location and Low Oscillating Shear Stress. *Arteriosclerosis* **1985**, *5*, 293–302.
2. Davies, P. F. Flow-Mediated Endothelial Mechanotransduction. *Physiol. Rev.* **1995**, *75*, 519–560.
3. Hahn, C.; Schwartz, M. A. Mechanotransduction in Vascular Physiology and Atherogenesis. *Nat. Rev. Mol. Cell Biol.* **2009**, *10*, 53–62.
4. Dewey, C. F.; Bussolari, S. R.; Gimbrone, M. A.; Davies, P. F. The Dynamic-Response of Vascular Endothelial-Cells to Fluid Shear-Stress. *J. Biomech. Eng.* **1981**, *103*, 177–185.
5. Harrison, D. G.; Widder, J.; Grumbach, I.; Chen, W.; Weber, M.; Searles, C. Endothelial Mechanotransduction, Nitric Oxide and Vascular Inflammation. *J. Int. Med.* **2006**, *259*, 351–363.
6. Hwang, J.; Saha, A.; Boo, Y. C.; Sorescu, G. P.; McNally, J. S.; Holland, S. M.; Dikalov, S.; Giddens, D. P.; Griendling, K. K.; Harrison, D. G.; et al. Oscillatory Shear Stress Stimulates Endothelial Production of O2- from P47phox-Dependent Nad(P)H Oxidases, Leading to Monocyte Adhesion. *J. Biol. Chem.* **2003**, *278*, 47291–47298.
7. Davis, M. E.; Grumbach, I. M.; Fukai, T.; Cutchins, A.; Harrison, D. G. Shear Stress Regulates Endothelial Nitric-Oxide Synthase Promoter Activity through Nuclear Factor KappaB Binding. *J. Biol. Chem.* **2004**, *279*, 163–168.
8. Widder, J. D.; Chen, W.; Li, L.; Dikalov, S.; Thony, B.; Hatakeyama, K.; Harrison, D. G. Regulation of Tetrahydrobiopterin Biosynthesis by Shear Stress. *Circ. Res.* **2007**, *101*, 830–838.
9. Nam, D.; Ni, C.-W.; Rezvan, A.; Suo, J.; Budzyn, K.; Llanos, A.; Harrison, D.; Giddens, D.; Jo, H. Partial Carotid Ligation Is a Model of Acutely Induced Disturbed Flow, Leading to Rapid Endothelial Dysfunction and Atherosclerosis. *Am. J. Physiol.: Heart Circ. Physiol.* **2009**, *297*, H1535–H1543.
10. Channon, K. M. Tetrahydrobiopterin: A Vascular Redox Target To Improve Endothelial Function. *Curr. Vasc. Pharmacol.* **2012**, *10*, 705–708.
11. Baigent, C.; Keech, A.; Kearney, P. M.; Blackwell, L.; Buck, G.; Pollicino, C.; Kirby, A.; Sourjina, T.; Peto, R.; Collins, R.; et al. Efficacy and Safety of Cholesterol-Lowering Treatment: Prospective Meta-Analysis of Data from 90056 Participants in 14 Randomised Trials of Statins. *Lancet* **2005**, *366*, 1267–1278.
12. Cannon, C. P.; Braunwald, E.; McCabe, C. H.; Rader, D. J.; Rouleau, J. L.; Belder, R.; Joyal, S. V.; Hill, K. A.; Pfeffer, M. A.; Skene, A. M.; et al. Intensive *versus* Moderate Lipid Lowering with Statins after Acute Coronary Syndromes. *N. Engl. J. Med.* **2004**, *350*, 1495–1504.
13. Peters, D.; Kastantin, M.; Kotamraju, V. R.; Karmali, P. P.; Gujraty, K.; Tirrell, M.; Ruoslahti, E. Targeting Atherosclerosis by Using Modular, Multifunctional Micelles. *Proc. Natl. Acad. Sci. U.S.A.* **2009**, *106*, 9815–9819.
14. Srinivasan, R.; Marchant, R. E.; Gupta, A. S. *In Vitro* and *In Vivo* Platelet Targeting by Cyclic Rgd-Modified Liposomes. *J. Biomed. Mater. Res., Part A* **2010**, *93*, 1004–1015.
15. Maiseyeu, A.; Mihai, G.; Kampfrath, T.; Simonetti, O. P.; Sen, C. K.; Roy, S.; Rajagopalan, S.; Parthasarathy, S. Gadolinium-Containing Phosphatidylserine Liposomes for Molecular Imaging of Atherosclerosis. *J. Lipid Res.* **2009**, *50*, 2157–2163.
16. Cai, J. O.; Liu, Z. F.; Wang, F.; Li, F. Phage Display Applications for Molecular Imaging. *Curr. Pharm. Biotechnol.* **2010**, *11*, 603–609.
17. Kelly, K. A.; Nahrendorf, M.; Yu, A. M.; Reynolds, F.; Weissleder, R. *In Vivo* Phage Display Selection Yields Atherosclerotic Plaque Targeted Peptides for Imaging. *Mol. Imaging Biol.* **2006**, *8*, 201–207.
18. Kelly, K. A.; Allport, J. R.; Tsourkas, A.; Shinde-Patil, V. R.; Josephson, L.; Weissleder, R. Detection of Vascular Adhesion Molecule-1 Expression Using a Novel Multimodal Nanoparticle. *Circ. Res.* **2005**, *96*, 327–336.
19. Hamzah, J.; Kotamraju, V. R.; Seo, J. W.; Agemy, L.; Fogal, V.; Mahakian, L. M.; Peters, D.; Roth, L.; Gagnon, M. K. J.; Ferrara, K. W.; et al. Specific Penetration and Accumulation of a Homing Peptide within Atherosclerotic Plaques of Apolipoprotein E-Deficient Mice. *Proc. Natl. Acad. Sci. U.S.A.* **2011**, *108*, 7154–7159.
20. Hallahan, D.; Geng, L.; Qu, S. M.; Scarfone, C.; Giorgio, T.; Donnelly, E.; Gao, X.; Clanton, J. Integrin-Mediated Targeting of Drug Delivery to Irradiated Tumor Blood Vessels. *Cancer Cell* **2003**, *3*, 63–74.
21. Son, D. J.; Kumar, S.; Takabe, W.; Kim, C. W.; Ni, C. W.; Alberts-Grill, N.; Jang, I. H.; Kim, S.; Kim, W.; Won Kang, S.; et al. The Atypical Mechanosensitive Microrna-712 Derived from Pre-ribosomal RNA Induces Endothelial Inflammation and Atherosclerosis. *Nat. Commun.* **2013**, *4*, 3000.
22. Bernatchez, P. N.; Acevedo, L.; Fernandez-Hernando, C.; Murata, T.; Chalouni, C.; Kim, J.; Erdjument-Bromage, H.; Shah, V.; Gratton, J. P.; Mcnally, E. M.; et al. Myoferlin Regulates Vascular Endothelial Growth Factor Receptor-2 Stability and Function. *J. Biol. Chem.* **2007**, *282*, 30745–30753.
23. Bernatchez, P. N.; Sharma, A.; Kodaman, P.; Sessa, W. C. Myoferlin Is Critical for Endocytosis in Endothelial Cells. *Am. J. Physiol.: Cell Physiol.* **2009**, *297*, C484–C492.
24. Sharma, A.; Yu, C.; Leung, C.; Trane, A.; Lau, M.; Utokaparch, S.; Shaheen, F.; Sheibani, N.; Bernatchez, P. A New Role for the Muscle Repair Protein Dysferlin in Endothelial Cell Adhesion and Angiogenesis. *Arterioscler., Thromb., Vasc. Biol.* **2010**, *30*, 2196–U2397.
25. Chidlow, J. H., Jr.; Sessa, W. C. Caveolae, Caveolins, and Cavins: Complex Control of Cellular Signalling and Inflammation. *Cardiovasc. Res.* **2010**, *86*, 219–225.
26. Fernandez-Hernando, C.; Yu, J.; Suarez, Y.; Rahner, C.; Davalos, A.; Lasuncion, M. A.; Sessa, W. C. Genetic Evidence Supporting a Critical Role of Endothelial Caveolin-1 during the Progression of Atherosclerosis. *Cell Metab.* **2009**, *10*, 48–54.
27. Conway, D. E.; Breckenridge, M. T.; Hinde, E.; Gratton, E.; Chen, C. S.; Schwartz, M. A. Fluid Shear Stress on Endothelial Cells Modulates Mechanical Tension across Ve-Cadherin and Pecam-1. *Curr. Biol.* **2013**, *23*, 1024–1030.
28. Orr, A. W.; Sanders, J. M.; Bevard, M.; Coleman, E.; Sarembock, I. J.; Schwartz, M. A. The Subendothelial Extracellular Matrix Modulates Nf-kappaB Activation by Flow: A Potential Role in Atherosclerosis. *J. Cell Biol.* **2005**, *169*, 191–202.
29. Orr, A. W.; Ginsberg, M. H.; Shattil, S. J.; Deckmyn, H.; Schwartz, M. A. Matrix-Specific Suppression of Integrin Activation in Shear Stress Signaling. *Mol. Biol. Cell* **2006**, *17*, 4686–4697.
30. Modarres, H. P.; Mofradt, M. R. Filamin: A Structural and Functional Biomolecule with Important Roles in Cell Biology, Signaling and Mechanics. *Mol. Cell Biomech.* **2014**, *11*, 39–65.
31. Schiller, C.; Diakopoulos, K. N.; Rohwedder, I.; Kremmer, E.; von Toerne, C.; Ueffing, M.; Weidle, U. H.; Ohno, H.; Weiss, E. H. Lst1 Promotes the Assembly of a Molecular Machinery Responsible for Tunneling Nanotube Formation. *J. Cell Sci.* **2013**, *126*, 767–777.
32. Stahlhut, M.; van Deurs, B. Identification of Filamin as a Novel Ligand for Caveolin-1: Evidence for the Organization

of Caveolin-1-Associated Membrane Domains by the Actin Cytoskeleton. *Mol. Biol. Cell* **2000**, *11*, 325–337.
33. Bachmann, A. S.; Howard, J. P.; Vogel, C. W. Actin-Binding Protein Filamin A Is Displayed on the Surface of Human Neuroblastoma Cells. *Cancer Sci.* **2006**, *97*, 1359–1365.
34. Sykes, M. C. Regulation of Endothelial Gene Transcription by Shear Stress in a Manner Dependent on P47phox-Based Nadph Oxidases. Ph.D. Dissertation, Georgia Institute of Technology, available from ProQuest Dissertations & Theses Full Text; ProQuest Dissertations & Theses Global, **2008**.
35. Glogauer, M.; Arora, P.; Chou, D.; Janmey, P. A.; Downey, G. P.; McCulloch, C. A. The Role of Actin-Binding Protein 280 in Integrin-Dependent Mechanoprotection. *J. Biol. Chem.* **1998**, *273*, 1689–1698.
36. Byfield, F. J.; Wen, Q.; Levental, I.; Nordstrom, K.; Arratia, P. E.; Miller, R. T.; Janmey, P. A. Absence of Filamin A Prevents Cells from Responding to Stiffness Gradients on Gels Coated with Collagen but Not Fibronectin. *Biophys. J.* **2009**, *96*, 5095–5102.
37. Psarros, C.; Lee, R.; Margaritis, M.; Antoniades, C. Nanomedicine for the Prevention, Treatment and Imaging of Atherosclerosis. *Nanomedicine* **2012**, *8*, S59–S68.
38. Farokhzad, O. C.; Langer, R. Impact of Nanotechnology on Drug Delivery. *ACS Nano* **2009**, *3*, 16–20.
39. Kirby, C.; Gregoriadis, G. Dehydration−Rehydration Vesicles: A Simple Method for High-Yield Drug Entrapment in Liposomes. *Nat. Biotechnol.* **1984**, *2*, 979–984.
40. Wang, S. S. para-Alkoxybenzyl Alcohol Resin and para-Alkoxybenzyloxycarbonylhydrazide Resin for Solid-Phase Synthesis of Protected Peptide Fragments. *J. Am. Chem. Soc.* **1973**, *95*, 1328–1333.
41. Sykes, E. A.; Chen, J.; Zheng, G.; Chan, W. C. W. Investigating the Impact of Nanoparticle Size on Active and Passive Tumor Targeting Efficiency. *ACS Nano* **2014**, *8*, 5696–5706.
42. Gabizon, A.; Papahadjopoulos, D. Liposome Formulations with Prolonged Circulation Time in Blood and Enhanced Uptake by Tumors. *Proc. Natl. Acad. Sci. U.S.A.* **1988**, *85*, 6949–6953.
43. Passman, J. N.; Dong, X. R.; Wu, S. P.; Maguire, C. T.; Hogan, K. A.; Bautch, V. L.; Majesky, M. W. A Sonic Hedgehog Signaling Domain in the Arterial Adventitia Supports Resident Sca1+ Smooth Muscle Progenitor Cells. *Proc. Natl. Acad. Sci. U.S.A.* **2008**, *105*, 9349–9354.
44. McNally, J. S.; Davis, M. E.; Giddens, D. P.; Saha, A.; Hwang, J.; Dikalov, S.; Jo, H.; Harrison, D. G. Role of Xanthine Oxidoreductase and Nad(P)H Oxidase in Endothelial Superoxide Production in Response to Oscillatory Shear Stress. *Am. J. Physiol.: Heart Circ. Physiol.* **2003**, *285*, H2290–H2297.
45. Landmesser, U.; Dikalov, S.; Price, S. R.; McCann, L.; Fukai, T.; Holland, S. M.; Mitch, W. E.; Harrison, D. G. Oxidation of Tetrahydrobiopterin Leads to Uncoupling of Endothelial Cell Nitric Oxide Synthase in Hypertension. *J. Clin. Invest.* **2003**, *111*, 1201–1209.
46. Shi, W.; Meininger, C. J.; Haynes, T. E.; Hatakeyama, K.; Wu, G. Regulation of Tetrahydrobiopterin Synthesis and Bioavailability in Endothelial Cells. *Cell Biochem. Biophys.* **2004**, *41*, 415–434.
47. Li, L.; Chen, W.; Rezvan, A.; Jo, H.; Harrison, D. G. Tetrahydrobiopterin Deficiency and Nitric Oxide Synthase Uncoupling Contribute to Atherosclerosis Induced by Disturbed Flow. *Arterioscler., Thromb., Vasc. Biol.* **2011**, *31*, 1547–1554.
48. Li, L.; Chen, W.; Rezvan, A.; Jo, H.; Harrison, D. G. Tetrahydrobiopterin Deficiency and Nitric Oxide Synthase Uncoupling Contribute to Atherosclerosis Induced by Disturbed Flow. *Arterioscler., Thromb., Vasc. Biol.* **2011**, *31*, 1547–1554.
49. Hasegawa, H.; Sawabe, K.; Nakanishi, N.; Wakasugi, O. K. Delivery of Exogenous Tetrahydrobiopterin (BH_4) to Cells of Target Organs: Role of Salvage Pathway and Uptake of Its Precursor in Effective Elevation of Tissue BH_4. *Mol. Genet. Metab.* **2005**, *86*, S2–S10.
50. Lanio, M. E.; Luzardo, M. C.; Alvarez, C.; Martinez, Y.; Calderon, L.; Alonso, M. E.; Zadi, B.; Gregoriadis, G.; Craig, D. Q.; Disalvo, A. Humoral Immune Response against Epidermal Growth Factor Encapsulated in Dehydration Rehydration Vesicles of Different Phospholipid Composition. *J. Liposome Res.* **2008**, *18*, 1–19.
51. Piedrahita, J. A.; Zhang, S. H.; Hagaman, J. R.; Oliver, P. M.; Maeda, N. Generation of Mice Carrying a Mutant Apolipoprotein-E Gene Inactivated by Gene Targeting in Embryonic Stem-Cells. *Proc. Natl. Acad. Sci. U.S.A.* **1992**, *89*, 4471–4475.
52. Plump, A. S.; Smith, J. D.; Hayek, T.; Aaltosetala, K.; Walsh, A.; Verstuyft, J. G.; Rubin, E. M.; Breslow, J. L. Severe Hypercholesterolemia and Atherosclerosis in Apolipoprotein-E-Deficient Mice Created by Homologous Recombination in Es Cells. *Cell* **1992**, *71*, 343–353.
53. Sanger, F.; Nicklen, S.; Coulson, A. R. DNA Sequencing with Chain-Terminating Inhibitors. *Proc. Natl. Acad. Sci. U.S.A.* **1977**, *74*, 5463–5467.
54. Nelson, C. E.; Kintzing, J. R.; Hanna, A.; Shannon, J. M.; Gupta, M. K.; Duvall, C. L. Balancing Cationic and Hydrophobic Content of PEGylated Sirna Polyplexes Enhances Endosome Escape, Stability, Blood Circulation Time, and Bioactivity *in Vivo*. *ACS Nano* **2013**, *7*, 8870–8880.
55. Fukushima, T.; Nixon, J. C. Analysis of Reduced Forms of Biopterin in Biological Tissues and Fluids. *Anal. Biochem.* **1980**, *102*, 176–188.
56. Fink, B.; Laude, K.; McCann, L.; Doughan, A.; Harrison, D. G.; Dikalov, S. Detection of Intracellular Superoxide Formation in Endothelial Cells and Intact Tissues Using Dihydroethidium and an HPLC-Based Assay. *Am. J. Physiol.: Cell Physiol.* **2004**, *287*, C895–902.